Neutron inelastic scattering study of the lattice dynamics of strontium titanate: harmonic models

1972 J. Phys. C: Solid State Phys. 5 2711

(http://iopscience.iop.org/0022-3719/5/19/005)

J. Phys. C: Solid State Phys., Vol. 5, 1972. Printed in Great Britain.

Neutron inelastic scattering study of the lattice dynamics of strontium titanate: harmonic models

W G STIRLING

University of Edinburgh, Department of Physics, James Clerk Maxwell Building, The King's Buildings, Mayfield Road, Edinburgh EH9 3JZ

MS received 25 May 1972

Abstract. Extensive neutron inelastic scattering measurements of the frequencies of normal modes in strontium titanate propagating in the crystallographic directions [0, 0, ζ], [ζ, ζ, 0], [ζ, ζ, ζ], [$\frac{1}{2}$, $\frac{1}{2}$, ζ] and [ζ, ζ, $\frac{1}{2}$] are reported. The temperature dependence of the 'soft' modes at points Γ and R have been investigated with particular emphasis on the mode of symmetry Δ_2, propagating in the direction [$\frac{1}{2}$, $\frac{1}{2}$, ζ]; quantitative estimates of the isotropy of the dispersion surface at Γ and R are given. Rigid ion, rigid shell, and deformable shell models of the crystal dynamics have been developed. Based on these, the frequency distribution, specific heat, one-phonon x ray scattering intensity, Debye–Waller factor, and two-phonon Raman spectrum have been calculated; where possible, these are compared with the available experimental measurements.

1. Introduction

Ferroelectric materials and their phase transitions have been studied in detail by many techniques, both experimental and theoretical. Strontium titanate has continued to be of particular interest because there are anomalously temperature dependent modes at both the Brillouin zone centre and zone corner. Measurements of the temperature dependence of the frequency of the lowest transverse optic mode at the zone centre by infrared (Spitzer *et al* 1962, Barker and Tinkham 1962) and by neutron scattering techniques (Cowley 1962a) provided the first direct experimental evidence for the 'soft mode' theory of Cochran (1960) for ferroelectrics. This crystal is not a ferroelectric, however, and the mode does not reach zero frequency (Worlock and Fleury 1967). A transition does occur at 105 K to a distorted phase as detected by electron paramagnetic resonance experiments (Müller *et al* 1968). This transition was found to be associated with an instability of the crystal against a zone corner R_{25} mode; the temperature dependence of this mode has been studied by light and neutron scattering methods (Fleury *et al* 1968, Shirane and Yamada 1969, Cowley *et al* 1969).

In parallel with this experimental work, theoretical studies of the near ferroelectric properties of $SrTiO_3$ were made by Silverman and Joseph (1964) and Cowley (1965). The 105 K transition has been treated theoretically by Slonczewski and Thomas (1970) and by Pytte and Feder (1969). All of these theories suggest that most of the temperature dependent behaviour could be understood in terms of the anharmonic interactions between the normal modes of vibration. The calculations suffered, however, in that the

nature of interatomic forces in $SrTiO_3$ was so imperfectly understood that various drastic simplifications and approximations had to be made. This paper describes the first part of a programme to attempt to rework these calculations using a more realistic model for the interatomic forces. In view of the recent realization of the importance of the critical effects (Müller *et al* 1970, Riste *et al* 1971), this programme is particularly appropriate as it will enable the detailed study of these effects with better microscopic models.

In the next section neutron inelastic scattering measurements are described of the frequencies of normal modes of vibration propagating in the $[0,0,\zeta]$, $[\zeta,\zeta,0]$, $[\zeta,\zeta,\zeta]$, $[\frac{1}{2},\frac{1}{2},\zeta]$ and $[\zeta,\zeta,\frac{1}{2}]$ crystallographic directions. These results are used to determine the parameters of lattice dynamical models for strontium titanate, based on the rigid ion model, rigid shell model, and deformable shell model. Since the models may be compared with a far greater quantity of experimental data than was available when earlier calculations were performed (Cowley 1964, hereafter referred to as I), the parameters of the models are expected to be more realistic and use of the models to extrapolate from and interpolate between the experimental results is certainly more reliable. A preliminary account of this work has been presented earlier (Stirling and Cowley 1972). The group theoretical notation introduced in I will be used throughout this paper.

In the second part of this work to be reported later it is intended to extend these models to include the anharmonic interactions and so to calculate the temperature dependence of the soft modes in detail.

2. The experiments

The experiments were performed by the method of neutron inelastic scattering using triple-axis crystal spectrometers (Brockhouse 1961) at the NRU reactor of AECL, Chalk River and the DIDO reactor of UKAEA, Harwell. The specimen used for both series of experiments was a large (4·7 cm in length, 1 cm minimum diameter) single crystal boule of strontium titanate kindly given by the National Lead Company, Titanium Division. For most of the experiments, the crystal was mounted with a $[\bar{1},1,0]$ axis vertical.

Measurements of the frequencies of the normal modes of vibration at room temperature were performed using the C4 spectrometer at Chalk River, with a fixed incident neutron energy of 18·2 meV. The 'constant $\boldsymbol{Q}$' and 'constant energy' techniques were employed in an energy gain configuration. In this way, low energy branches of the dispersion relation, with polarization vectors consistent with the crystal alignment, were measured for the symmetry directions listed in § 1. The C5 spectrometer, operating in an energy loss configuration, was used to measure phonon frequencies up to 15 THz, at 90 K. The crystal, in the same orientation as described above, was mounted in a cryostat. 'Constant $\boldsymbol{Q}$' and 'constant energy' scans were carried out using neutrons of variable incident energy and fixed scattered energies of 32·7 and 28·6 meV. Use was made of the eigenvectors and mode structure factors of I to enable a choice to be made of reciprocal lattice point, and hence the momentum transfer $\boldsymbol{Q}$, at which a particular mode might best be observed.

The data collected in this way, along with those of I for the $[0,0,\zeta]$ direction, are shown in figure 1, where both 297 K and 90 K measurements are indicated. For comparison, a few points obtained by Cowley *et al* (1969) and Shirane and Yamada (1969) are shown. The temperature dependence of the frequency of the zone centre Γ_{15} and

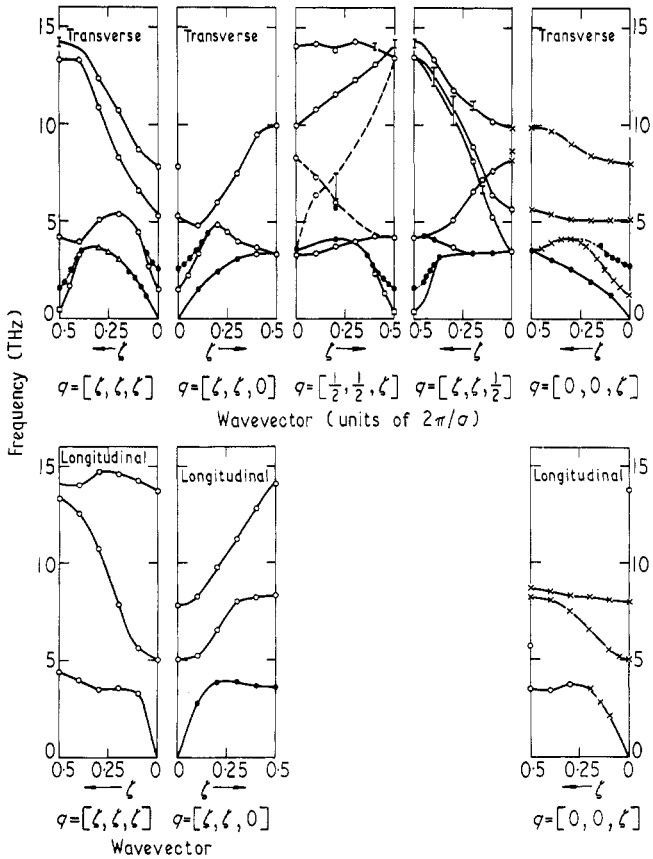

Figure 1. Experimentally determined dispersion curves of $SrTiO_3$ at 297 K and 90 K. The lines are guides to the eye. ○ 90 K; ● 297 K; × 90 K, Cowley (1964); △ 300 K Cowley *et al* (1969); □ 120 K Shirane and Yamada (1969).

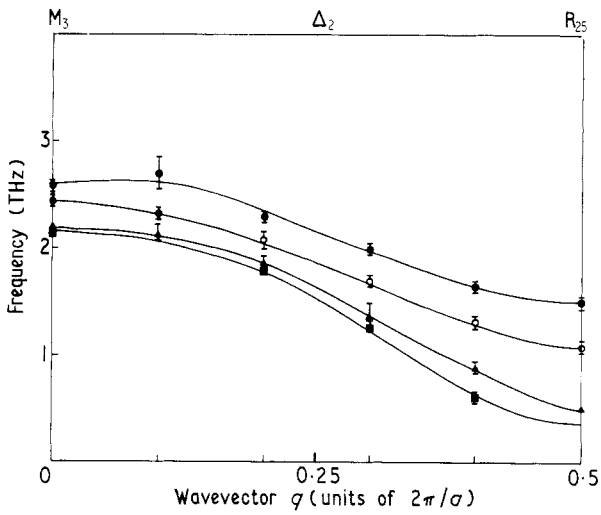

Figure 2. Temperature dependence of the frequency of normal mode Δ_2 of $SrTiO_3$ propagating in direction $[\frac{1}{2}, \frac{1}{2}, \zeta]$. The lines are guides to the eye. ● 297 K, ○ 201 K, ▲ 118 K, ■ 78 K.

Table 1. Experimentally determined normal mode frequencies (THz) at 297 K for principal symmetry points. Also shown are the corresponding results for models 4, 5 and 6 with the irreducible representations assigned on the basis of these models. Only those symmetry labels which differ from model to model are given.

Longitudinal

Point	Model					
$\Gamma(0,0,0)$	Experiment	0	5·08 ± 0·10	7·95 ± 0·15	13·70 ± 0·50	24·70 ± 0·30
	4	0	5·03	8·08	12·67	24·61
		(Γ_{15})	(Γ_{15})	(Γ_{25})	(Γ_{15})	(Γ_{15})
	5	0	5·10	8·27	14·75	21·91
	6	0	5·16	8·45	14·80	21·28
$X(0,0,\frac{1}{2})$	Experiment	3·45 ± 0·15	8·20 ± 0·20	8·70 ± 0·15	—	—
	4	3·77	8·93	10·03	15·59	22·57
		($M_{2'}$)	(M_3)	(M_1)	(M_1)	($M_{2'}$)
	5	4·07	9·00	9·22	18·04	19·97
			(M_1)	(M_3)		
	6	3·98	9·24	9·35	17·81	18·60
$M(\frac{1}{2},\frac{1}{2},0)$	Experiment	3·60 ± 0·15	8·40 ± 0·20	14·05 ± 0·25	—	—
	4	3·49	8·94	13·44	14·14	25·27
		($M_{5'}$)	($M_{5'}$)	($M_{5'}$)	(M_1)	(M_4)
	5	3·26	8·95	13·30	14·56	21·57
				(M_1)	($M_{5'}$)	
	6	3·17	8·79	13·26	13·38	19·99
$R(\frac{1}{2},\frac{1}{2},\frac{1}{2})$	Experiment	1·55 ± 0·06	4·36 ± 0·12	13·50 ± 0·20	14·20 ± 0·50	—
	4	1·78	3·65	12·43	13·57	26·41
		(R_{25})	(R_{15})	(R_{15})	($R_{25'}$)	($R_{2'}$)
	5	1·76	3·72	12·65	14·49	22·14
	6	1·73	3·84	12·76	12·77	20·53

Transverse

Point	Model										
$\Gamma(0,0,0)$	Experiment	0	2·75 ± 0·09	5·08 ± 0·10	7·95 ± 0·15	16·40 ± 0·10					
	4	0	2·52	5·04	8·08	16·20					
		(Γ_{15})	(Γ_{15})	(Γ_{15})	(Γ_{25})	(Γ_{15})					
	5	0	2·56	5·17	8·27	16·76					
	6	0	2·65	5·21	8·45	17·07					
$X(0,0,\frac{1}{2})$	Experiment	3·55 ± 0·05	3·55 ± 0·05	5·88 ± 0·08	9·85 ± 0·20	—					
	4	3·66	3·69	5·94	9·19	15·26					
		($M_{5'}$)	(M_5)	(M_5)	($M_{5'}$)	(M_5)					
	5	3·59	3·65	6·03	9·31	16·50					
		(M_5)	($M_{5'}$)								
	6	3·63	3·68	6·21	9·30	16·81					
		($M_{5'}$)	(M_5)								
$M(\frac{1}{2},\frac{1}{2},0)$	Experiment	2·63 ± 0·05	3·33 ± 0·12	—	3·33 ± 0·12	—	9·95 ± 0·20	9·95 ± 0·20	—	—	—
	4	1·95	2·86	3·49	3·65	8·94	9·54	9·54	12·97	13·44	13·78
		(M_3)	($M_{3'}$)	($M_{5'}$)	($M_{2'}$)	($M_{5'}$)	(M_5)	(M_5)	(M_2)	($M_{5'}$)	($M_{3'}$)
	5	2·01	3·24	3·26	3·63	8·95	9·14	9·14	12·52	14·56	16·10
	6	1·98	2·85	3·17	3·62	8·79	9·12	9·12	11·82	13·38	16·50
$R(\frac{1}{2},\frac{1}{2},\frac{1}{2})$	Experiment	1·55 ± 0·06	4·36 ± 0·12	13·50 ± 0·20	13·40 ± 0·40	—					
	4	1·78	3·65	12·43	12·89	13·57					
		(R_{25})	(R_{15})	(R_{15})	($R_{12'}$)	($R_{25'}$)					
	5	1·76	3·72	12·44	12·65	14·49					
				($R_{12'}$)	(R_{15})						
	6	1·73	3·84	11·75	12·76	12·77					

zone corner R_{25} modes is clearly seen. The branch of symmetry Δ_2 propagating in direction $[\frac{1}{2},\frac{1}{2},\zeta]$ is not shown here but in figure 2. The frequencies observed for the high symmetry points in the Brillouin zone at 297 K are listed in table 1.

The mode, propagating in the zone-edge direction $[\frac{1}{2},\frac{1}{2},\zeta]$, of symmetry Δ_2 was studied at a series of temperatures from room temperature to 78 K, using the triple-axis crystal spectrometer at the DIDO reactor of UKAEA, Harwell. This mode was observed by mounting the crystal with a $[\bar{1},3,0]$ axis vertical; the temperature was held constant to about ± 1 K. Harmonic models of the crystal dynamics (described below) based on the experimental data obtained at Chalk River, indicated that this mode was unstable against small changes in the force constants. The results show (figure 2) that the entire branch decreases in frequency with decreasing temperature and, moreover, exhibits little dispersion. This mode thus seems to provide an anisotropic feature of the dispersion surface about the R point of the zone; similar behaviour has been observed for this mode in the isomorphous material $KMnF_3$ (Shirane 1972, Gesi *et al* 1972). In this material the condensation of the M_3 mode precipitates a structural phase transition at 91·5 K, but no evidence of such behaviour has been observed for $SrTiO_3$. Measurements of the intensity of the elastic scattering at points along the direction $[\frac{1}{2},\frac{1}{2},\zeta]$, using a germanium analysing crystal to minimize $\lambda/2$ contamination, failed to show any temperature dependence over the temperature range studied.

To determine the degree of isotropy of the dispersion surface, the modes in the neighbourhood of the zone centre Γ_{15} and zone corner R_{25} modes were studied. In the neighbourhood of these points, wavevector $\boldsymbol{q}_0$, the dispersion relation may be written as

$$\omega^2(\boldsymbol{q}j) = \omega^2(\boldsymbol{q}_0 j) + \Lambda_j(\hat{\boldsymbol{p}})\,|\boldsymbol{q} - \boldsymbol{q}_0|^2$$

where $\hat{\boldsymbol{p}}$ is a unit vector in the direction of $\boldsymbol{q} - \boldsymbol{q}_0$. In table 2 the values of the Λ_j are listed for the directions measured at two different temperatures for $SrTiO_3$ and, for

Table 2. Values of the parameter $\Lambda_j(\hat{p})$ obtained experimentally for the dispersion curves in the neighbourhood of the Γ_{15} and R_{25} modes of $SrTiO_3$ compared with the corresponding results for $BaTiO_3$ and $KMnF_3$ (units of (THz Å)^2).

Point Γ. Neighbourhood of mode Γ_{15}

	$SrTiO_3$ 90 K	$SrTiO_3$ 297 K	$BaTiO_3$ 423 K
Δ_5	110 ± 12	98 ± 10	57
Σ_4	189 ± 12	108 ± 8	57
Λ_3	255 ± 23	151 ± 15	278

Point R. Neighbourhood of mode R_{25}

	$SrTiO_3$ 90 K	$SrTiO_3$ 297 K	$KMnF_3$ 295 K
Δ_5 (T_5)	216 ± 20	205 ± 27	42
Σ_1 (S_1)	139 ± 23	112 ± 22	18
Λ_3	139 ± 15	131 ± 23	26
Δ_2 (T_2)	7 ± 2	8 ± 2	≃0

comparison, the analogous results for the zone centre mode of $BaTiO_3$ (Harada *et al* 1971) and the R_{25} mode of $KMnF_3$ (Gesi *et al* 1972). The dispersion surface in $SrTiO_3$ is seen to be less anisotropic for the Γ_{15} mode than in $BaTiO_3$ while the behaviour at the zone corner is similar to that in $KMnF_3$. Particularly at the R point, the results also indicate that the $\Lambda_j(\hat{\boldsymbol{p}})$ are relatively temperature independent. Recently Schwabl (1972) and von Waldkirch *et al* (1972) have used an approximate form for the $\Lambda_j(\hat{\boldsymbol{p}})$ coefficients around the R point in $SrTiO_3$. They write

$$\Lambda_j(\hat{\boldsymbol{p}}) = \alpha^2\{1 - (1 - \Delta)\,\hat{p}_z^2\}$$

Our results are not entirely satisfactorily described by this form, but if $\alpha = 14{\cdot}4$ (THz Å) and $\Delta = 0{\cdot}0354$, the experimental frequencies are described approximately. This value of Δ is, however, considerably larger than that (0·017) suggested by von Waldkirch *et al* (1972).

3. The models

3.1. Theory

The normal mode frequencies obtained in the experiments described above were used to obtain the parameters of several harmonic models of the crystal dynamics. The simplest model considered for the inter-ion interactions is the rigid ion (RI) model (Kellermann 1940) in which the ionic polarizability is neglected. For this model, the equation of motion is then

$$M_\kappa\omega^2(\boldsymbol{q}j)\,\boldsymbol{u}(\kappa\boldsymbol{q}j) = \sum_{\kappa'}\{R_{\kappa\kappa'}(\boldsymbol{q}) + Z_\kappa C_{\kappa\kappa'}(\boldsymbol{q})\,Z_{\kappa'}\}\,\boldsymbol{u}(\kappa'\boldsymbol{q}j)$$

for atom κ, charge Z_κ, displacement $\boldsymbol{u}(\kappa\boldsymbol{q}j)$ in mode j. Axially symmetric short range interactions were considered to act between strontium and oxygen, titanium and oxygen, and oxygen and oxygen nearest neighbours as indicated in figure 3. The elements of matrix $R_{\kappa\kappa'}(\boldsymbol{q})$, which contains terms describing such interactions, are as listed in I. Values for the coefficients $C_{\kappa\kappa'}(\boldsymbol{q})$, describing the Coulomb interaction of charges Z_κ and $Z_{\kappa'}$, were

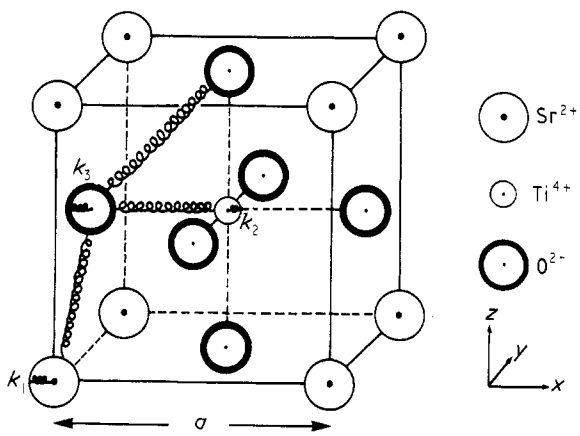

Figure 3. Structure of $SrTiO_3$ with nearest neighbour short range interactions indicated. Also shown are shell core couplings, k_κ.

obtained by the method of Ewald (Born and Huang 1954). This model has then eight adjustable parameters, six for short range interactions and two for ionic charges (Z_{oxygen} was fixed by charge neutrality).

The model may be extended to allow for polarization of the ions, the rigid shell (RS) model (Woods *et al* 1960). In this work the same approximations were employed as by Woods *et al* (1960); namely, short range forces effectively act between neighbouring shells. The equations of motion for this model may be expressed as

$$M_\kappa \omega^2(\boldsymbol{q}j)\, \boldsymbol{u}(\kappa \boldsymbol{q}j) = \sum_{\kappa'} \{R_{\kappa\kappa'}(\boldsymbol{q}) + Z_\kappa C_{\kappa\kappa'}(\boldsymbol{q})\, Z_{\kappa'}\}\, \boldsymbol{u}(\kappa' \boldsymbol{q}j) + \sum_{\kappa'} \{R_{\kappa\kappa'}(\boldsymbol{q}) + Z_\kappa C_{\kappa\kappa'}(\boldsymbol{q})\, Y_{\kappa'}\}\, \boldsymbol{w}(\kappa' \boldsymbol{q}j)$$

$$0 = \sum_{\kappa'} \{R_{\kappa'\kappa}(\boldsymbol{q}) + Y_\kappa C_{\kappa\kappa'}(\boldsymbol{q})\, Z_{\kappa'}\}\, \boldsymbol{u}(\kappa' \boldsymbol{q}j) + \sum_{\kappa'} \{S_{\kappa\kappa'}(\boldsymbol{q}) + Y_\kappa C_{\kappa\kappa'}(\boldsymbol{q})\, Y_{\kappa'}\}\, \boldsymbol{w}(\kappa' \boldsymbol{q}j)$$

Here the relative shell-core displacement is described by vector $\boldsymbol{w}(\kappa \boldsymbol{q}j)$ while the short range matrix $S_{\kappa\kappa'}(\boldsymbol{q})$ contains terms arising from the coupling constants k_κ for a particular ionic core and shell; as in the RI model, matrix products such as ZCZ contain self-terms due to the translational invariance of the lattice. The model has then 14 adjustable parameters, the same short range and ionic charge parameters as the RI model while, in addition, the ionic polarizability is described by two parameters for each ion; α_κ, the electrical polarizability and d_κ, the short range polarizability.

These quantities were defined as in I, namely

$$\alpha_\kappa = \frac{Y_\kappa^2}{k_\kappa + (R_{\kappa\kappa})_0} \qquad d_\kappa = -\frac{Y_\kappa (R_{\kappa\kappa})_0}{k_\kappa + (R_{\kappa\kappa})_0}$$

$(R_{\kappa\kappa})_0$ are the diagonal elements of matrix $R_{\kappa\kappa'}(\boldsymbol{q})$ at $\boldsymbol{q} = 0$.

In an attempt to improve upon the RS model, Schröder (1966) has suggested that the formalism be extended to allow for radial deformation of the shells. The resulting deformable shell (DS) model has proved to be very successful for dynamical models of the alkali halides (eg Schröder 1966, Nusslein and Schröder 1967), and for MgO (Sangster *et al* 1970). An additional force constant, coupling the ion core to the shell, is used to describe radial deformations of each ion. The equations of motion are thus an extended form of those of the RS model and may be written,

$$M_\kappa \omega^2(\boldsymbol{q}j)\, \boldsymbol{u}(\kappa \boldsymbol{q}j) = \sum_{\kappa'} \{R_{\kappa\kappa'}(\boldsymbol{q}) + Z_\kappa C_{\kappa\kappa'}(\boldsymbol{q})\, Z_{\kappa'}\}\, \boldsymbol{u}(\kappa' \boldsymbol{q}j) + \sum_{\kappa'} \{R_{\kappa\kappa'}(\boldsymbol{q}) + Z_\kappa C_{\kappa\kappa'}(\boldsymbol{q})\, Y_{\kappa'}\}\, \boldsymbol{w}(\kappa' \boldsymbol{q}j) + \sum_{\kappa'} \boldsymbol{Q}_{\kappa\kappa'}(\boldsymbol{q})\, \boldsymbol{v}(\kappa' \boldsymbol{q}j)$$

$$0 = \sum_{\kappa'} \{R_{\kappa'\kappa}(\boldsymbol{q}) + Y_\kappa C_{\kappa\kappa'}(\boldsymbol{q})\, Z_{\kappa'}\}\, \boldsymbol{u}(\kappa' \boldsymbol{q}j) + \sum_{\kappa'} \{S_{\kappa\kappa'}(\boldsymbol{q}) + Y_\kappa C_{\kappa\kappa'}(\boldsymbol{q})\, Y_{\kappa'}\}\, \boldsymbol{w}(\kappa' \boldsymbol{q}j) + \sum_{\kappa'} \boldsymbol{Q}_{\kappa\kappa'}(\boldsymbol{q})\, \boldsymbol{v}(\kappa' \boldsymbol{q}j)$$

$$0 = \sum_{\kappa'} \boldsymbol{Q}^*_{\kappa'\kappa}(\boldsymbol{q}) \{\boldsymbol{u}(\kappa' \boldsymbol{q}j) + \boldsymbol{w}(\kappa' \boldsymbol{q}j)\} + \sum_{\kappa'} H_{\kappa\kappa'}(\boldsymbol{q})\, \boldsymbol{v}(\kappa' \boldsymbol{q}j)$$

The matrix $\boldsymbol{v}(\kappa \boldsymbol{q}j)$ has then 5 elements describing the radial deformations of the 5 atoms in the unit cell of $SrTiO_3$. Matrix $\boldsymbol{Q}_{\kappa\kappa'}(\boldsymbol{q})$ describes interactions between radial and translational shell deformations while $H_{\kappa\kappa'}(\boldsymbol{q})$ involves interactions between radial shell deformations.

3.2. Results

In the models reported here, fitting was carried out for wavevectors at the zone centre, the zone boundary in the three directions [0,0,ζ], [ζ,ζ,0] and [ζ,ζ,ζ], and an intermediate point in each of these directions. To supplement the neutron results, zone centre optic mode frequencies obtained by infrared spectrometry (Spitzer *et al* 1962, Barker and Tinkham 1962) were also fitted. Thus a total of 48 normal mode frequencies were normally used to obtain the model parameters. The inclusion of further phonon frequencies resulted in very little change in the parameters.

Most of the experimental frequencies were determined at 90 K, but within the experimental error, the only differences obtained between normal mode frequencies measured at 90 K and 297 K were found to occur for the modes Γ_{15}, R_{25} and Δ_2, discussed in § 2. Thus, models fitted to '297 K' data used the 90 K frequencies except where appreciable differences had been measured. Consequently, figures 4 and 5, which give fitted dispersion curves for 297 K models, show frequencies determined at 90 K with the exceptions discussed above.

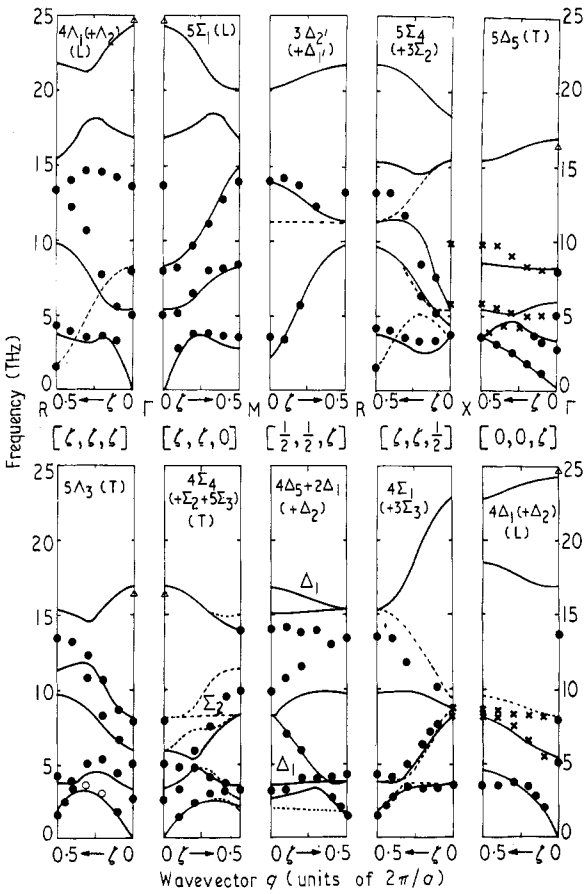

Figure 4. Fitted dispersion curves of $SrTiO_3$ (297 K) for model 1. ● present results; × Cowley (1964); △ infrared frequencies. Irreducible representations observable with a $[\bar{1},1,0]$ crystallographic axis vertical are shown as full lines; others are shown as broken lines and appear in brackets. Purely longitudinal modes are labelled L, pure transverse T.

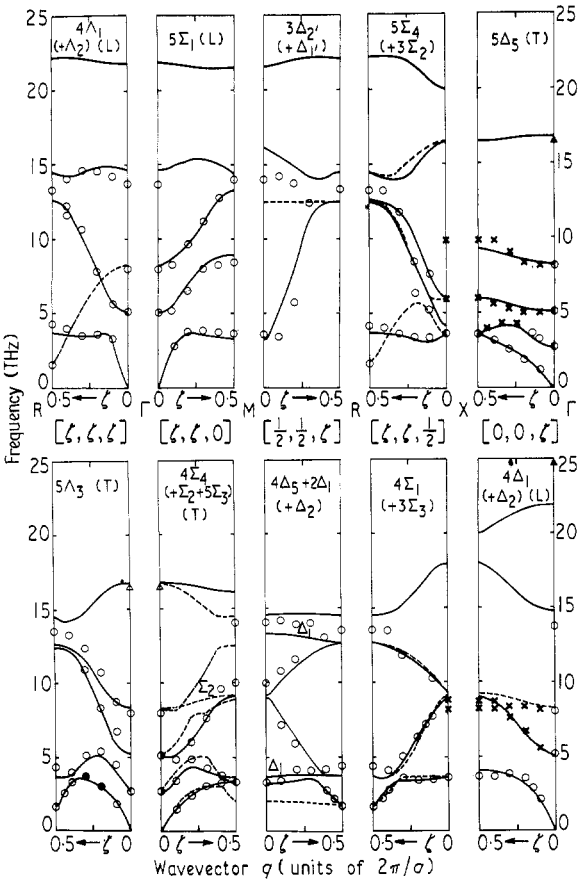

Figure 5. Fitted dispersion curves of $SrTiO_3$ (297 K) for model 5, displayed as in figure 4. The present data are here denoted ○.

With the eigenvectors† given in I, block diagonalization of the dynamical matrix (see, for example, Chen 1967) was carried out for each value of $\boldsymbol{q}$ used in the fitting; this procedure results in a minimization of computation time as the largest matrix to be diagonalized is then of order 5 rather than of order 15 if the complete dynamical matrix were employed.

† The displacements of the ions for modes Λ_3, quoted in I, are not quite correct. A set of basis vectors for modes Λ_3, compatible with those at the R point, are given below:

$$\Lambda_3: \tfrac{1}{2}\mathrm{Sr}_x = -\mathrm{Sr}_y = -\mathrm{Sr}_z$$

$$\tfrac{1}{2}\mathrm{Ti}_x = -\mathrm{Ti}_y = -\mathrm{Ti}_z$$

$$\tfrac{1}{2}\mathrm{O}_{\mathrm{III}x} = -\mathrm{O}_{\mathrm{II}y} = -\mathrm{O}_{\mathrm{I}z}$$

$$\tfrac{1}{2}\mathrm{O}_{\mathrm{I}y} = -\mathrm{O}_{\mathrm{I}x} = -\mathrm{O}_{\mathrm{II}x} = \tfrac{1}{2}\mathrm{O}_{\mathrm{II}z} = -\mathrm{O}_{\mathrm{III}y} = -\mathrm{O}_{\mathrm{III}z}$$

$$\mathrm{O}_{\mathrm{I}x} = \mathrm{O}_{\mathrm{II}x} = -\mathrm{O}_{\mathrm{III}y} = -\mathrm{O}_{\mathrm{III}z}$$

$$\Lambda_3: \mathrm{Sr}_z = -\mathrm{Sr}_y \qquad \mathrm{Ti}_z = -\mathrm{Ti}_y \qquad \mathrm{O}_{\mathrm{II}y} = -\mathrm{O}_{\mathrm{I}z}$$

$$\mathrm{O}_{\mathrm{I}x} = -\mathrm{O}_{\mathrm{II}x} = -\mathrm{O}_{\mathrm{III}y} = \mathrm{O}_{\mathrm{III}z}$$

$$\mathrm{O}_{\mathrm{I}x} = \tfrac{1}{2}\mathrm{O}_{\mathrm{I}y} = -\mathrm{O}_{\mathrm{II}x} = -\tfrac{1}{2}\mathrm{O}_{\mathrm{II}z} = \mathrm{O}_{\mathrm{III}y} = -\mathrm{O}_{\mathrm{III}z}$$

The fitted dispersion curves for the RI model, model 1, at 297 K, are shown in figure 4, while the parameters for this model, fitted to data at 297 K and 90 K are given in table 3. The models fitted to the 90 K results neglected any effect of the 105 K structural phase transition. As can be seen, the fit is fairly good except for the $[\zeta,\zeta,\zeta]$ direction, considering the simplicity of the model. In particular, phonon frequencies predicted by the model for the zone boundary directions $[\frac{1}{2},\frac{1}{2},\zeta]$ and $[\zeta,\zeta,\frac{1}{2}]$ are in reasonable agreement with experiment. These directions were not normally involved in the fitting procedure. Fixing

Table 3. The parameters of the models. Parameters which were held constant during fitting are marked*; in models 3 to 6, only the short range force parameters were allowed to vary when fitting the 90 K data from the 297 K parameters. No calculated errors in the parameters are given as in general, small changes in the force constants produced relatively small changes in the calculated frequencies except for the anomalously temperature dependent modes discussed in the text. Values of χ^2 are given where N_0 is number of observations and N_v is number of variable parameters.

Short range forces (units of $e^2/2v$)							*Ionic charges (e)*	
Model		Strontium–oxygen		Titanium–oxygen		Oxygen–oxygen	Strontium	Titanium
		A_1	B_1	A_2	B_2	A_3 B_3	Z_1	Z_2
297 K	1	13·75	−0·49	200·08	−61·57	−1·26 4·05	1·09	3·68
	2	23·13	0·80	274·13	−59·51	−5·00 2·42	2·00*	4·00*
	3	46·73	−0·23	256·23	−53·29	−6·56 2·05	3·00	3·59
	4	7·41	1·72	344·42	−67·67	8·60 −1·32	0·58	4·96
	5	20·81	0·14	322·77	−76·22	1·95 1·96	1·54	4·62
	6	28·58	−3·13	311·55	−84·51	2·62 2·76	1·46	4·59
90 K	1	14·33	−1·81	202·21	−63·30	−1·54 4·73	1·09*	3·68*
	2	23·14	0·78	273·90	−59·39	−4·99 2·43	2·00*	4·00*
	3	47·78	0·77	256·71	−55·04	−6·78 2·38	3·00*	3·59*
	4	8·22	1·20	346·22	−67·78	8·57 −1·28	0·58*	4·96*
	5	23·59	−1·39	324·60	−79·32	1·82 2·45	1·54*	4·62*
	6	34·62	−6·33	317·35	−91·41	1·71 3·78	1·46*	4·59*

Ionic polarizability ($10^{-24} cm^3$)				*Short range polarizability (e)*			
Model	Strontium	Titanium	Oxygen	Strontium	Titanium	Oxygen	χ^2†
	α_1	α_2	α_3	d_1	d_2	d_3	
1	—	—	—	—	—	—	39·8 (297 K) 45·8 (90 K)
297 K 2	0·0190	0·00293	0·0299	−0·588	−0·053	0·724	38·5 (297 K)
90 K 2	0·0205	0·00321	0·0299	−0·613	−0·0522	0·723	33·5 (90 K)
297 K & 3	0·025*	0·003*	0·040*	−1·117	−0·085	1·030	29·4 (297 K)
90 K							24·0 (90 K)
297 K & 4	0·025	0·068	0·018	−0·030	−2·013	0·561	16·1 (297 K)
90 K							13·0 (90 K)
297 K & 5	0·025	0·003	0·027	−0·669	0·010	0·809	15·0 (297 K)
90 K							11·5 (90 K)
297 K & 6	0·028	−0·006	0·027	−0·791	0·190	0·805	33·0 (297 K)
90 K							20·0 (90 K)

Deformable shell parameter, G_3, model 6: 6204·9 (e^2/v)

† $\chi^2 = \sum \frac{1}{N_0 - N_v + 1} \left(\frac{\omega_{obs}^2 - \omega_{calc}^2}{2\omega_{obs} \Delta\omega_{obs}} \right)^2$

the ionic charges at their 'free ion' values resulted in a poor fit so Z_1 and Z_2 were allowed to vary freely. All the ionic charges are seen to be reduced from the free ion values—the oxygen charge for model 1 is $-1{\cdot}59$ (e)—a fact which is no doubt due to the neglect of ionic polarizability. The parameters of this model at 297 K were allowed to vary to fit the 90 K frequencies and, in common with the more complex models, the temperature dependence of the unstable modes Γ_{15} and R_{25} could be obtained with only relatively small changes in the short range force constants. It proved impossible, however, to reproduce simultaneously the temperature dependence of R_{25} and of mode M_3 at $(\frac{1}{2}, \frac{1}{2}, 0)$—see figure 2. Possible inclusion of anharmonic effects is required to reproduce this feature. Indeed, when only Γ_{15} and R_{25} were fitted, the frequency of M_3 was predicted to be very much smaller than that found experimentally. Some models produced an imaginary value for this mode frequency. One other feature of this model is of interest. In common with the models of I, by far the largest short range forces would appear to act between the titanium and oxygen ions.

The best fit to the observed frequencies was obtained using the rigid shell model of which models 2 to 5 are examples. In model 2 the ionic charges were kept fixed at their nominal values and the agreement is seen to be improved over that of the RI model, there being 12 variable parameters in this shell model. As can be seen in table 3, the value of the short range polarizability for Sr is large and negative. This feature of shell model calculations has often been observed, for instance in the alkali halide RS models of Cowley *et al* (1963), and has been explained as due to the neglect of ionic deformations in the model. Once again, in common with *all* the models reported here, Ti–O short range forces are very much larger than the others. All twelve parameters of the 297 K model were allowed to vary in fitting the 90 K data although little change resulted in the polarizabilities. Consequently it was decided in subsequent models to allow only the parameters A_i and B_i to vary when different temperatures were being considered.

Model 3 was further constrained by fitting to experimental values of the high frequency dielectric constant, ϵ^∞ (Levin *et al* 1955), and the elastic constants C_{11}, C_{12}, C_{44} (Bell and Rupprecht 1963), calculated as described by Cowley (1962b). Even when constrained to fit these quantities, the model values for the elastic constants and dielectric constant are only in fair agreement with experiment (table 4). The values of α_κ were kept fixed at those obtained by Tessman *et al* (1953), while ionic charges were free to vary. Agreement with experiment is further improved although the ionic charges are seen to assume values considerably different from those of free ions—table 3. (The value of Z_{oxygen} is $-2{\cdot}20$ (e) for this model.)

Models 4 and 5 are also examples of the RS model in which ϵ^∞ and C_{ij} were not fitted and in which all parameters were allowed to vary freely. In this way, much better agreement with the experimentally determined normal mode frequencies was obtained although the two sets of parameters are very different. Large negative values of d are seen to occur for positive ions in both models. Model 4 was able to provide a value of the frequency of the highest frequency $q = 0$ optic mode in better agreement with that measured by infrared techniques (approximately 24·7 THz) than that of model 5. The ionic charges of model 4 are very different from those of free ions whilst those of model 5 are more reasonable. The oxygen charges are $-1{\cdot}85$ (e) and $-2{\cdot}05$ (e) respectively. Moreover, the overall agreement provided by model 5 was slightly better and thus this model was used as a basis for most subsequent calculations. In figure 5 are shown the fitted dispersion curves for this model. The fact that both of the different sets of parameters of models 4 and 5 give reasonable agreement with experiment emphasizes the difficulty of extracting reliable force constants from experimental dispersion curves. Such a model does, however, give a

fairly reliable interpolation scheme for calculating frequencies at non symmetry points throughout the Brillouin zone.

Although in models of the alkali halides (Schröder 1966, Nüsslein and Schröder 1967) the extra force constant introduced in the DS model is normally set equal to that for translational motion of the negative shell, this need not be so. Indeed, Sangster *et al* (1970) have shown that for MgO much poorer results are obtained with this assumption. Similar behaviour has been observed in DS models for $SrTiO_3$, the best fit being found when isotropic radial deformations of the oxygen ions alone were allowed with the G_3 force constant varying freely in the least squares fitting. This model, model 6, did not, however, produce any improvement over other simpler shell models attempted. It proved very difficult to achieve convergence of the least squares procedure, the best fit being obtained starting with the parameters of model 5. Further attempts to obtain a stable model in which radial deformation of more than one ion was allowed also proved unsatisfactory. It is thought that, to describe more correctly the anisotropic oxygen polarizability, it may be necessary to extend the model to allow for anisotropic deformable shell coupling constants; this, however, adds yet more variable parameters and is not considered worthwhile.

Table 4. Calculated elastic and dielectric constants. The experimental values quoted for the elastic constants are from Bell and Rupprecht (1963), ϵ^{∞} from Levin *et al* (1955), and ϵ^{0} from Mitsui and Westphal (1961). ϵ' was calculated explicitly and ϵ^{0} calculated from this as described by Cochran and Cowley (1962).

Model	Elastic constants (10^{12} dyn cm^{-2})			Dielectric constants	
	C_{11}	C_{12}	C_{44}	ϵ^{0}	ϵ^{∞}
297 K Experiment	3·30	1·01	1·24	301·0	5·5
1	2·33	0·83	0·76	42·4	1·0
2	2·95	0·71	1·67	228·7	3·4
3	3·58	0·89	2·24	265·5	4·7
4	4·44	0·94	1·21	485·9	8·4
5	3·61	1·28	1·65	183·0	3·3
90 K Experiment	3·35	1·05	1·27	1305·0	5·5
1	2·37	0·96	0·68	222·4	1·0
2	2·94	0·70	1·67	745·7	3·4
3	3·63	0·98	2·20	750·0	4·7
4	4·50	1·02	1·19	2069·2	8·6
5	3·73	1·55	1·56	612·6	3·4

In table 1, the normal mode frequencies calculated with models 4, 5, and 6 at 297 K are compared with experimental values obtained for the points Γ, R, X and M of the Brillouin zone. The different models produce very similar frequencies except for the highest frequency optic modes which are very model dependent. In general, only the temperature dependent modes discussed above yielded significantly different frequencies between the 297 K and 90 K models. It is of interest to note that the steep dip in the dispersion surface about the R point is reproduced by these *harmonic* models. Values of the elastic constants and dielectric constants for the simpler models are compared with the experimental values in table 4. The high frequency dielectric constant was calculated

explicitly and the low frequency constant obtained from this by use of the Lyddane–Sachs–Teller relation as extended by Cochran and Cowley (1962). For a cubic crystal, the 'equilibrium condition'

$$\left(\frac{\delta U}{\delta r}\right)_{r=R_0} = 0$$

where U is the crystal energy, gives that $C_{12} = C_{44}$. This is not the case, however, for the DS model (see, for example, Sangster *et al* 1970). Experimentally this relation is seen to be incorrect for $SrTiO_3$ although model 5 at 90 K appears to satisfy this condition.

4. Calculations with the models

4.1. Frequency distribution and specific heat

Using the models described above the frequencies and eigenvectors of normal modes were calculated for wavevectors throughout the Brillouin zone. Calculations were carried out for wavevectors (h,k,l) $0{\cdot}1(2\pi/a)$ where $h \leqslant 5$, $k \leqslant h$, $l \leqslant k$ (integers h, k, l). Phonon frequencies for all other such points in the Brillouin zone were obtained by symmetry. With this mesh of wavevectors the frequency distribution of normal modes, $g(\nu)$, was obtained. The distribution for model 5 is shown in figure 6, where calculations based on

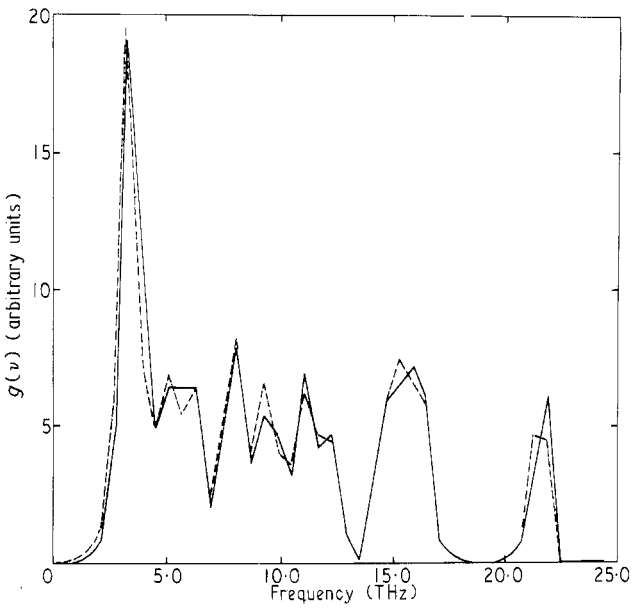

Figure 6. Frequency distribution of normal modes of $SrTiO_3$ for model 5 at 297 K (full curve) and 90 K (broken curve).

both 297 K and 90 K models are displayed. Very similar frequency distributions were obtained using energy 'bin sizes' ranging from 0·2 to 0·6 THz. The results shown are for $\Delta E = 0{\cdot}6$ THz, chosen so that the error in the calculated $g(\nu)$ is consistent with the average error of the experimental results. Distributions for models 4 and 6 have much the same structure as that reported except that model 4 produces a peak in $g(\nu)$ at about 25·6 THz, considerably higher than that of models 5 and 6.

Calculated values of C_V, the lattice specific heat at constant volume, as a function of temperature, are compared with the experimental data of Todd and Lorenson (1952)—see figure 7. Their heat capacities at constant pressure have been corrected using the coefficient of linear expansion measured by Lytle (1964). More recent measurements (Hegenbarth 1962, Lombardo *et al* 1965) over the range 4 K to 40 K indicate a T^3 behaviour for the specific heat of $SrTiO_3$. The calculations presented here are, unfortunately, not sufficiently accurate to verify this as the extrapolation to low temperatures is not justified considering the data on which the models are based.

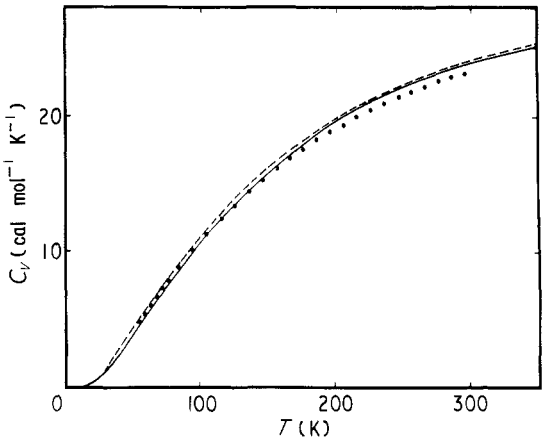

Figure 7. Lattice specific heat of $SrTiO_3$ calculated using model 4 at 297 K (full curve) and model 5 at 90 K (broken curve) compared with experiment (●).

4.2. One-phonon x ray scattering intensity

The intensity of one-phonon thermal diffuse x ray scattering is obtained from (Cochran 1963):

$$\left(\frac{d\sigma}{d\Omega}\right)^{(1)} = \sum_{\kappa} \frac{NQ^2}{M_\kappa} \sum_{j=1}^{3s} \frac{E(\boldsymbol{q}j)}{\omega^2(\boldsymbol{q}j)} |F_j(\boldsymbol{Q})|^2$$

where

$$E(\boldsymbol{q}j) = \{n(\boldsymbol{q}j) + \tfrac{1}{2}\}\,\hbar\omega(\boldsymbol{q}j)$$

$$QF_j(\boldsymbol{Q}) = \boldsymbol{Q} \cdot \sum_{\kappa} \boldsymbol{e}(\kappa\boldsymbol{q}j) f(\kappa\boldsymbol{Q}) \exp\{i\,\boldsymbol{G} \cdot \boldsymbol{r}(\kappa)\}$$

with

$$\boldsymbol{Q} = \boldsymbol{G} + \boldsymbol{q}$$

The factor $f(\kappa\boldsymbol{Q})$ contains the Debye–Waller factor $\exp(-B(\kappa)\sin^2\theta/\lambda^2)$ but this was considered to be a constant in the calculation. Interpolated values of the ionic scattering factors $f_0(\kappa\boldsymbol{Q})$ were calculated based on the atomic scattering factors obtained from the *International Tables for X ray Crystallography* (1962). Normalized eigenvectors $\boldsymbol{e}(\kappa\boldsymbol{q}j)$ and the eigenfrequencies $\omega(\boldsymbol{q}j)$ were calculated for models 4, 5 and 6. The intensity was calculated for a series of reciprocal lattice vectors $\boldsymbol{G}$ throughout several Brillouin

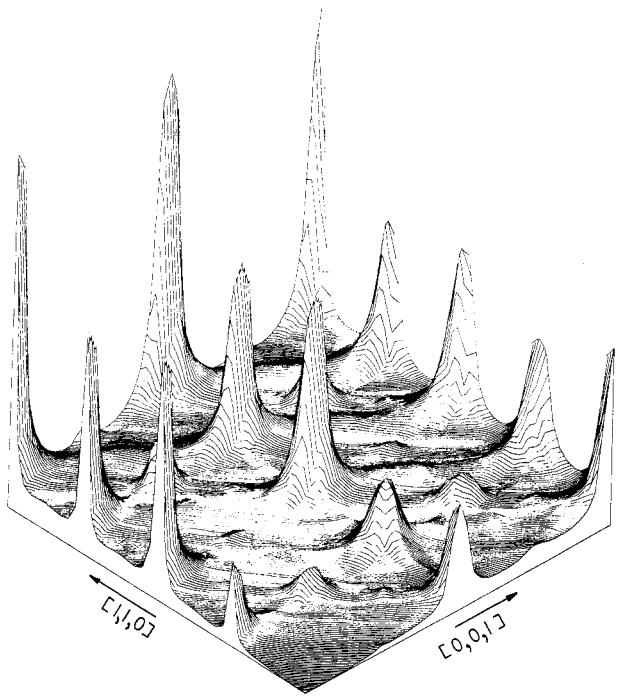

Figure 8. Calculated one-phonon thermal diffuse x ray scattering intensity for model 5 (297 K). Intensity is plotted vertically for a $(\bar{1},1,0)$ reciprocal lattice plane.

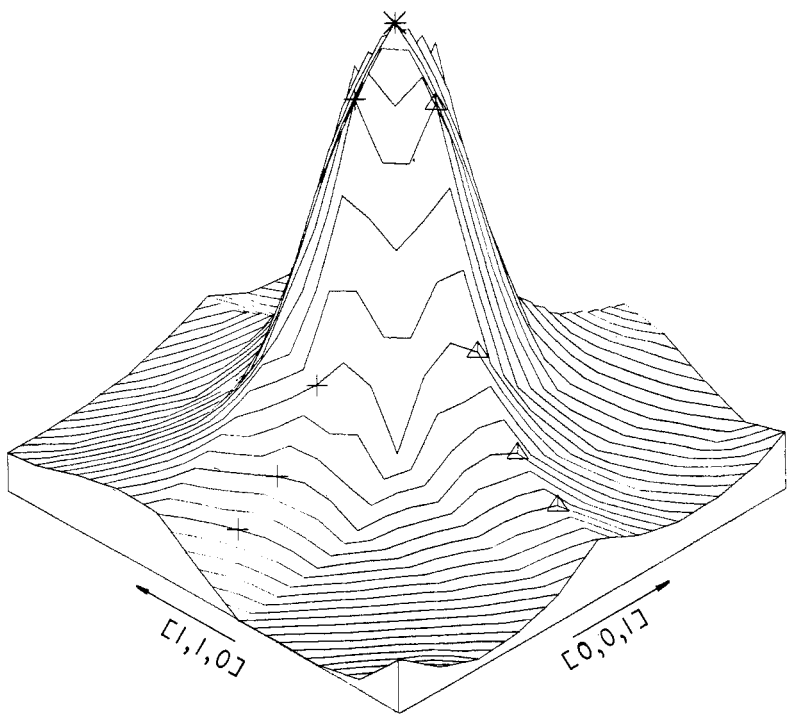

Figure 9. Enlarged portion of figure 8 in the neighbourhood of reciprocal lattice point (1,1,2), marked*.

zones of the reciprocal lattice to obtain the x ray scattering intensity for both the (0,0,1) and $(\bar{1},1,0)$ planes of reciprocal space.

Numerical results for the models used indicate ridges of intensity along principal symmetry directions. A two dimensional smoothed computer plot of the calculated intensity (plotted vertically) for model 5 shows these features clearly (figure 8). Reciprocal lattice points out to (4,4,4) are shown as the peaks where the intensity was interpolated arbitrarily. Figure 9 gives an enlarged portion of this diagram. The region of the reciprocal lattice plane $(\bar{1},1,0)$ about the point (1,1,2) is shown with the points marked on directions $[0,0,\zeta]$ and $[\zeta,\zeta,0]$ at which the calculation was performed.

A well defined ridge is seen in the latter direction while a less definite increase is indicated for direction $[0,0,\zeta]$. All three models used as a basis for these calculations produced similar results.

'Streaks' of intensity have been observed in the isomorphous perovskite materials $BaTiO_3$, $KNbO_3$ (Comes *et al* 1968) and $KTa_xNb_{1-x}O_3$ (Zaccai 1972). The present calculations are consistent with (1,0,0) planes of intensity even though in § 3 it was shown that the anisotropy in the dispersion curves for $SrTiO_3$ is relatively small. Similar calculations have recently been published for $KMnF_3$ (Gesi *et al* 1972), based on an approximate form of the dynamical matrix around the R point. These authors come to the similar conclusion that the anisotropy in diffuse x ray scattering can arise from the particular form of the dispersion surface. It is intended to attempt these calculations for $BaTiO_3$ and other perovskites, but there is at present insufficient neutron scattering data to produce realistic models of the crystal dynamics.

4.3. The Debye–Waller factor

The coefficient $B(\kappa)$ of the Debye–Waller factor $\exp\{-B(\kappa)\sin^2\theta/\lambda^2\}$ may be expressed (Dolling *et al* 1965) as

$$B(\kappa) = \frac{4\pi^2}{3}\left(\frac{\hbar}{NM_\kappa}\right)\sum_{\boldsymbol{q}j\alpha}\frac{|e_\alpha(\kappa\boldsymbol{q}j)|^2}{\omega(\boldsymbol{q}j)}\{2n(\boldsymbol{q}j)+1\}$$

Table 5. Calculated temperature factors $B(\kappa)$, Å^2, for models 4, 5 and 6 compared with experimentally determined values for $BaTiO_3$.

Temperature (K)	Model	B(Sr)	B(Ti)	$B(O_1)$	$B(O_2)$
100	4 (90)	0·199	0·135	0·194	0·402
	5 (90)	0·208	0·155	0·185	0·397
	6 (90)	0·228	0·194	0·195	0·399
300	4 (297)	0·492	0·251	0·278	0·807
	5 (297)	0·511	0·303	0·258	0·790
	6 (297)	0·526	0·352	0·275	0·783
	$BaTiO_3$ experiment	B(Ba)	B(Ti)	$B(O_1)$	$B(O_2)$
300	Evans (4)	0·27	0·42	0·43	0·49
	Evans (5)	0·27	0·41	0·57	0·90
	Harada (D)	0·47	0·29	0·55	0·49

This coefficient has been calculated for models 4, 5 and 6, summing over the 56 $\boldsymbol{q}$ vectors, suitably weighted, described in §4.2. Preliminary calculations indicated that only a small error was introduced by ignoring the three $\boldsymbol{q} = 0$ uniform translations of the crystal. In table 5 are shown the results, at two temperatures, for the Sr, Ti and the two nonequivalent oxygen ions in the unit cell. For comparison, values obtained from models 4 and 5 of Evans (1961) based on x ray diffraction measurements and model D of Harada *et al* (1970), using neutron diffraction techniques, are included in the table. Both these

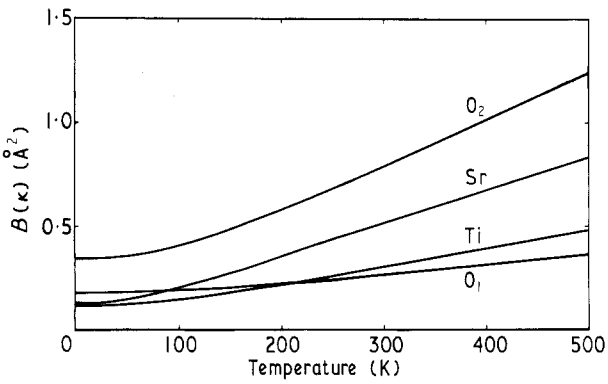

Figure 10. Calculated temperature factors of $SrTiO_3$, $B(\kappa)$, as a function of temperature for model 5 (297 K).

structure determinations are for tetragonal $BaTiO_3$ and the comparison with cubic $SrTiO_3$ is made by taking $(2B_{11} + B_{33})/3$ for Ba and Ti, $(2B_{11}(O_2) + B_{33}(O_1))/3$ for O_1 and $(B_{22}(O_2) + B_{33}(O_2) + B_{11}(O_1))/3$ for O_2. In this way a direct comparison is possible and the calculated results for $SrTiO_3$ are seen to be similar to those of the quoted models for $BaTiO_3$. It is interesting to note the large difference in $B(\kappa)$ between the two oxygens, O_1 which corresponds to motion in the Ti–O plane and O_2 in the Sr–O plane. The average amplitude of the latter motion is by far the greater; this may be understood qualitatively when one considers the perovskite structure, as an oxygen motion in the Ti–O plane must, of necessity, be more constrained than a motion in the Sr–O plane. Further, the models indicate that the Ti–O forces are considerably larger than those between strontium and oxygen. Figure 10 displays the calculated temperature dependence of $B(\kappa)$ for model 5. Above about 200 K, all four coefficients vary approximately linearly with temperature.

4.4. Two-phonon Raman spectrum

Above the 105 K structural phase transition, the Raman spectrum of $SrTiO_3$ is wholly second order. Nielsen and Skinner (1968) have recorded the spectrum measured in the $X(YY)Z$ configuration at various temperatures; recently these measurements have been repeated at room temperature (Arthur 1972 private communication). The second order Raman spectrum for this configuration has been calculated using the model developed for ionic crystals by Bruce and Cowley (1972). I am grateful to Mr A Bruce for assistance with this calculation. The frequencies and eigenvectors, for both translational and radial

shell deformations, were calculated for model 6 throughout the Brillouin zone; only those contributions to the Raman spectrum arising from deformations of the oxygen ions were considered in a two-parameter model. Preliminary results of these calculations are shown in figure 11. The principal features of the experimentally observed spectrum are present in the model calculations. It is intended to perform further experiments and calculations for other polarizations.

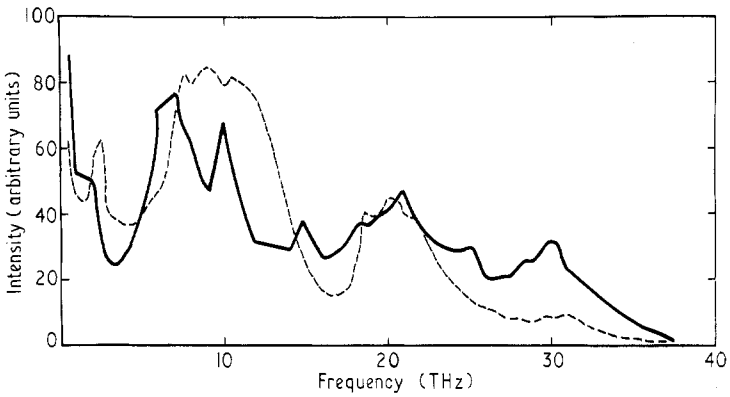

Figure 11. Calculated two-phonon $X(YY)Z$ Raman spectrum of $SrTiO_3$ (full curve) based on DS model 6 (297 K), compared with experimentally observed spectrum (broken curve).

Acknowledgments

The author wishes to thank the Science Research Council for the award of a Studentship and, along with Atomic Energy of Canada Ltd, for making available experimental facilities. I am most grateful for the continued help and encouragement of Professor R A Cowley. I should also like to thank Professor W Cochran for many useful discussions on this work, Dr H Montgomery who provided valuable guidance on group theoretical matters, and Dr R S Katiyar for help with the early parts of the calculations. General thanks are also due to my colleagues at Edinburgh, Chalk River and Harwell.

References

Barker A S and Tinkham M 1962 *Phys. Rev.* **125** 1527–30
Bell R O and Rupprecht G 1963 *Phys. Rev.* **129** 90–4
Born M and Huang K 1954 *Dynamical Theory of Crystal Lattices* (London: Oxford UP) pp 385–7
Brockhouse B N 1961 *Inelastic Scattering of Neutrons in Solids and Liquids* (Vienna: IAEA) pp 113–24
Bruce A D and Cowley R A 1972 *J. Phys.* C: *Solid St. Phys.* **5** 595–605
Chen S H 1967 *Phys. Rev.* **163** 532–46
Cochran W 1960 *Adv. Phys.* **9** 387–423
—— 1963 *Rep. Prog. Phys.* **26** 1–43
Cochran W and Cowley R A 1962 *J. Phys. Chem. Solids* **23** 447–50
Comes R, Lambert M and Guinier A 1968 *C.R. Acad. Sci., Paris* **266** 959–62
Cowley R A 1962a *Phys. Rev. Lett.* **9** 159–61
—— 1962b *Proc. R. Soc.* A **268** 121–43
—— 1964 *Phys. Rev.* **134** A981–97
—— 1965 *Phil. Mag.* **11** 673–706

Cowley R A, Buyers W J L and Dolling G 1969 *Solid St. Commun.* **7** 181–4
Cowley R A, Cochran W, Brockhouse B N and Woods A D B 1963 *Phys. Rev.* **131** 1030–9
Dolling G, Cowley R A and Woods A D B 1965 *Can. J. Phys.* **43** 1397–413
Evans H T 1961 *Acta. Crystallogr.* **14** 1019–26
Fleury P A, Scott J F and Worlock J M 1968 *Phys. Rev. Lett.* **21** 16–9
Gesi K, Axe J D, Shirane G and Linz A 1972 *Phys. Rev.* B **5** 1933–41
Harada J, Pedersen T and Barnea Z 1970 *Acta. Crystallogr.* A **26** 336–44
Harada J, Axe J D and Shirane G 1971 *Phys. Rev.* B **4** 155–62
Hegenbarth E 1962 *Phys. Stat. Solidi* **2** 1544–51
International Tables for X ray Crystallography 1962 (Birmingham: Kynoch Press) pp 201–12
Kellerman E W 1940 *Phil. Trans. R. Soc.* A **238** 513–48
Levin S B, Field N J, Plock F M and Merker L 1955 *J. Opt. Soc. Am.* **45** 737–9
Lombardo G, Sievers A J and Pohl R O 1965 *Bull. Phys. Soc.* **10** 44
Lytle F W 1964 *J. appl. Phys.* **35** 2212–5
Mitsui T and Westphal W B 1961 *Phys. Rev.* **124** 1354–9
Müller K A, Berlinger W and Waldner F 1968 *Phys. Rev. Lett.* **21** 814–7
Müller K A, Berlinger W and Slonczewski J C 1970 *Phys. Rev. Lett.* **25** 734–7
Nielsen W G and Skinner J G 1968 *J. chem. Phys.* **48** 2240–8
Nüsslein V and Schröder U 1967 *Phys. Stat. Solidi* **21** 309–14
Pytte E and Feder J 1969 *Phys. Rev.* **187** 1077–88
Riste T, Samuelsen E J, Otnes K and Feder J 1971 *Solid St. Commun.* **9** 1455–8
Sangster M J L, Peckham G and Saunderson D H 1970 *J. Phys.* C: *Solid St. Phys.* **3** 1026–36
Schröder U 1966 *Solid St. Commun.* **4** 347–9
Schwabl F 1972 *Phys. Rev. Lett.* **28** 500–3
Shirane G 1972 *Proc. NATO Advanced Study Institute on Structural Phase Transitions, Geilo, Norway* to be published
Shirane G and Yamada Y 1969 *Phys. Rev.* **177** 858–63
Silverman B D and Joseph R I 1964 *Phys. Rev.* **133** A207–10
Slonczewski J C and Thomas H 1970 *Phys. Rev.* B **1** 3599–608
Spitzer W G, Miller R C and Kleinman D A 1962 *Bull. Am. Phys. Soc.* **7** 280
Stirling W G and Cowley R A 1972 *Proc. 2nd European Conf. on Ferroelectricity, Dijon, 1971* to be published
Tessman J R, Kahn A H and Shockley W 1953 *Phys. Rev.* **92** 890–5
Todd S S and Lorenson R E 1952 *J. Am. Chem. Soc.* **74** 2043–5
von Waldkirch T, Müller K A, Berlinger W and Thomas H 1972 *Phys. Rev. Lett.* **28** 503–6
Woods A D B, Cochran W and Brockhouse B N 1960 *Phys. Rev.* **119** 980–99
Worlock J M and Fleury P A 1967 *Phys. Rev. Lett.* **19** 1176–9
Zaccai G 1972 *Proc. 2nd European Conference on Ferroelectricity, Dijon, 1971* to be published